25 Bone Response to Laser Microtextured Surfaces

J.L. Ricci, J. Charvet, S.R. Frenkel, R. Chang, P. Nadkarni, J. Turner, and H. Alexander

Tissue response to any implantable device has been found to correlate with a complex combination of material interface parameters based on composition, surface chemistry, and surface microgeometry. The relative contributions of these factors are difficult to assess.

In vitro and in vivo experiments have demonstrated the role of surface microgeometry in tissue-implant surface interaction although no well-defined relationship has been established. The general relationship, as demonstrated by in vivo experiments on metallic and ceramic implants [1-10] indicates that smooth surfaces promote formation of thick fibrous tissue encapsulation and rough surfaces promote thinner soft tissue encapsulation and more intimate bone integration. Smooth and porous titanium surfaces have also been shown to have different effects on the orientation of fibrous tissue cells in vitro [11,12]. Surface roughness has been shown to be a factor in tissue integration of implants with hydroxyapatite surfaces [4, 8], and to alter cell attachment and growth on polymer surfaces roughened by hydrolytic etching [13]. Roughened surfaces have also shown pronounced effects on differentiation and regulatory factor production of bone cells in vitro [14,15]. Defined surface microgeometries, such as grooved and machined metals and polymer surfaces [11, 16-19] have been shown to cause cell and ECM orientation in vivo and can be used to encourage or impede epithelial downgrowth in experimental dental implants [9]. Surface texturing has also been shown to adhere fibrin clot matrix more effectively than smooth surfaces [20], forming a more stable interface during the collagenous matrix contracture that occurs during healing. This is an effect which may be important in determining early events in tissue integration.

It is likely that textured surfaces work on several levels. These surfaces have higher surface areas than smooth surfaces and interdigitate with tissue in such a way as to create a more stable mechanical interface. They may also have significant effects on adhesion of fibrin clot, adhesion of more permanent extracellular matrix components, and long-term interaction of cells at stable interfaces. We have observed that, in the short term, fibrous tissue cells form an earlier and more organized collagenous capsule at smooth interfaces than at textured interfaces. We suggest that textured surfaces have an additional advantage over smooth surfaces. They inhibit colonization by fibroblastic cell types that arrive early in wound healing and encapsulate smooth substrates.

We have investigated (1) the effects of textured surfaces on colony formation by fibroblasts, and (2) the effects of controlled surface microgeometries on fibroblast colonization. Based on these results we have designed, fabricated, and tested titanium alloy and commercially-pure titanium implants with controlled microgeometries in in vivo models. These experimental surfaces have highly-oriented, consistent microstructures which are applied using computer-controlled laser ablation techniques. The results suggest that controlled surface microgeometry, in specific size ranges, can enhance bone integration and control the local microstructural geometry of attached bone.

Materials and Methods

In Vitro Studies

Production of Textured Culture Surfaces. Standard petri plates (not surface treated for cell attachment) were fitted with masks which covered 1/2 of their surfaces. They were then aluminum oxide grit blasted using a compressed-air-powered blast system and air pressure parameters designed to produce surface microtexturing in the size range of surfaces used on commercial orthopaedic implants. Fresh blast medium was used to ensure that no additional elements or materials were added to the blast textured surfaces during processing. The surfaces were then sonicated to remove adherent

Pre-edited copy of
Chapter 25 in: *Bone Engineering* [ed; JE Davies] to be published by Em^2 Inc., Toronto, Canada.

blast medium and cleaned with detergent. They were then evaporation-coated with titanium oxide in a Denton 502 Vacuum Evaporator. To obtain a 600 angstrom coating, the substrates were placed 100mm from a tungsten basket electrode containing commercially pure titanium foil, and the electrode was powered at 40kW while the chamber was under $5x10^{-5}$mtorr vacuum. They were then sterilized in 70% ethanol and dried in a sterile hood before use. It is important to note that experimental textures and smooth controls were contained on the same surface in the same dish, and that both were exposed to the same cleaning solutions, vapor deposition treatments, and sterilization techniques.

Production of Surfaces with Defined Microgeometries. Microtextured surfaces used in this study consisted of well-characterized unidirectionally oriented (microgrooved) structures of selected sizes and geometries. Grooves were fabricated to have square wave profiles, a shape that has been demonstrated to exert a strong cellular contact guidance effect [18]; flat surfaces (produced by the same methods) served as controls.

Following the nomenclature of Cheroudi et al. [11] the distance comprising one groove and one ridge between the grooves is called the repeat spacing, or pitch. The depth of the groove refers to its deepest point, and the width is the total opening in the plane of the substrate. It was expected that the greatest microgeometric effect on cells would be observed in the 2- to 12-um region that approximately brackets the size of the cell body in different attachment states.

The substrates used in these experiments have been molded from templates that were precision-fabricated at the Cornell Nanofabrication Facility at Cornell University (CNF). Mold surfaces were fabricated from silicon substrates using photomasking, microlithography, and reactive ion etching techniques. Surfaces were made with 2, 4, 6, 8, and 12 μm groove width and depth (4, 8, 12, 16, and 24 μm repeat spacing). Because of reactive ion etching limitations, the 12 μm surfaces (24 μm repeat spacing) were etched only to 8 μm depth.

The finished templates were attached to three inch aluminum rods by epoxy to produce a rigid base. Each circular template was constructed with one-half consisting of an experimental microgeometry surface and one-half consisting of a flat control.

Polystyrene culture plate surfaces were created from the templates by solvent casting. The mold solution was obtained by dissolving 15g of petri plate polystyrene in 100mL ethyl acetate for at least six hours. A dam was produced by attaching tape around the perimeter of the template. An 8mm solvent depth produced 0.5mm-thick polystyrene substrates. After pouring the solvent on the template and before allowing it to dry, they were placed under high vacuum for 1 minute to eliminate air bubbles at the interface. The solvent was allowed to dry for 24 hours and were then placed in a water bath for 5 hours. The substrates were peeled from their respective templates and their outer edges were removed to yield 50mm circular plates. The substrates were allowed to dry for 24 hours or more to completely remove the solvent.

They were then evaporation-coated using the same technique described for the textured surfaces. Prior to the start of the experiment each surface was ethanol-sterilized and tacked to a culture plate using a heated probe. Surfaces were characterized using scanning electron microscopy.

Preparation of Rat Tendon Fibroblast (RTF) Cell Cultures from Explants. To initiate RTF cell cultures, hindfoot extensor tendons were removed from male, 14-day-old Sprague-Dawley rats that had been sacrificed by Halothane overdose. Four extensor tendons were removed under sterile conditions from each foot and placed in Hank's balanced salt solution (HBSS) containing 1% penicillin-streptomycin. These tendons were then separated from sheath tissue by microdissection. All culture procedures were conducted under sterile conditions. Explant cultures were grown in a 37°C incubator in an atmosphere consisting of 95% air, 5% CO_2, and saturated humidity. These cultures were maintained with Dulbecco's Modified Eagle's Medium (DMEM) containing 10% fetal bovine serum and 1% penicillin-streptomycin. The medium was carefully maintained at pH 7.4 . Cells were subcultured at confluence and the explants were discarded. Only first, second, and third passage cells were used in experiments.

Initiation of Cell Colonies. Radiating "dot" cultures of RTF cells in a collagenous matrix were used as a surface colonization model. These cultures were initiated by mixing cell suspensions with pepsin-digested type I bovine collagen solution (Vitrogen 100, Collagen Corporation). This solution is dispensed as 2-ul aliquots (containing 20,000 cells each) on the control and experimental substrates and polymerized to form gels. Eight colonies were formed on each 60-mm-diameter textured/control culture plate or 50-mm-diameter cast substrate (designed to fit in a 60-mm culture plate) with four colonies on the experimental side (with microtexturing or microgeometry) and four colonies on the control (flat) side. The resulting gel "dots" acted as sources of cells for colony formation. The cultures were

maintained under standard sterile conditions in previously-described medium. In both in vitro studies colonies were also initiated on standard culture plates as additional controls.

Analysis of Surface Colonization. Cultures were examined using a Wild inverted-phase contrast microscope with Olympus 35mm camera attachment. In this model, colony formation begins from a circular dot of cell-containing collagen gel. Cell migrate and proliferate out from the gel forming circular colonies that grow at consistent rates on control surfaces.

RTF cell colonies were grown on each of the experimental and control substrates listed earlier. Eight colonies of each cell type were initiated on each surface (control and experimental) at each time period (four and eight days). They were measured for area, diameter (on non-directional microtextured and control surfaces), x-axis growth (parallel to surface microgeometry), and y-axis growth (perpendicular to surface microgeometry). In order to correct for small variations in initial colony size and shape, average colony parameters at 4 days were subtracted from the 8-day data for each cell type and surface. This yields data expressed as area, x-axis, or y-axis increase between 4 and 8 days.

RTF cell colony densities (in cells/mm^2), cell attachment areas (measuring individual cell spreading), and cell eccentricities (measuring long/short axis ratios, a measure of cell elongation) were also measured. This was done to determine effects of differences in the surface areas and configurations of the substrates on individual cell behavior. Cell densities were measured in multiple regions of the dense, internal areas of the cell colonies, where cell populations were stable. Most growth in these colonies was observed to occur at the periphery where cell density is low and cells are actively migrating and proliferating.

In Vivo Studies.

Experimental Design. Two models were used to text bone response to laser microtextured implants. An experimental implant chamber system was used to compare bone response to three types of surfaces; laser micromachined implant surfaces with 12 μm groove size (24 μm repeat spacing) produced from commercially-pure titanium (MG12), grit blasted titanium alloy (gA), and grit blasted commercially pure titanium (gCP). These three surfaces were also produced with preset coatings of medical grade calcium sulfate cement (see "Biological Mechanisms of Calcium Sulfate Replacement by Bone") for testing in the same model. These samples were designated MG12/CS, gA/CS, and gCP/CS. Twelve skeletally mature large canines were used in this study and 120 samples were tested at 3, 6, and 12 weeks.

A canine intramedullary (IM) rod model was also used to test cylindrical specimens of the MG12 (produced in circumferential and longitudinal orientations) and gCP surfaces, as well as polished commercially pure titanium (pCP). Each IM rod consisted of a central mounting rod and six stacked cylinders containing the test surfaces. In each animal two IM rods were placed, one in each hind femur. One rod contained the MG12 samples (both orientations) and the other contained the gCP and pCP specimens. Three animals (six rods, 36 specimens) were used in this study.

The Implantable Chamber System. used in this study has been described in "Biological Mechanisms of Calcium Sulfate Replacement by Bone" [21,22] and used to test a number of materials including other textured metal surfaces, hydroxyapatite surfaces, polymer surfaces, and resorbable polymer materials [21-22]. This system was designed to evaluate bone and soft tissue response to experimental materials. In this method we surgically placed two experimental chambers in each canine. Each chamber contained 10 test specimens and was implanted in a bone window cut in the distal lateral femur. This system allowed testing of bone and soft tissue response to up to 20 experimental samples in each canine.

Canine Intramedullary Rod Model. A canine IM rod model was also used to test laser microtextured specimens. In this model a modular IM rod, consisting of test cylinders stacked on a central mounting rod with threaded end caps, was placed in the intramedullary canal of an intact femur (no fracture). These samples were surgically placed in the central third of the femur using an approach through the trochanteric fossa of the hip. This model was used to examine longer-term response to these experimental surfaces at 3 and 6 months.

Fabrication of Laser Micromachined Implants. Microgroove patterns were produced on flat and cylindrical commercially-pure titanium samples. These were produced using a pulsed, computer-controlled Excimer laser system and large-area masking techniques. Controlled sample motion coupled with pulsed laser ablation was used to produce microgrooved patterns based on the results of the cell culture studies. Samples with MG12 surfaces, gCP and gA samples (produced using standard grit blasting methods), and pCP samples were then cleaned using organic solvents, sonicated in detergent solution, and passivated in nitric

acid according to industry standard ASTM protocols, before autoclave sterilization and implantation.

Evaluation of Tissue Response.

Faxitron Histomorphometry of Bone Penetration. Faxitron high-resolution x-ray images were used to document bone ingrowth into the implantable chambers. These images of the intact chambers showed the furthest extent of bone penetration into each channel. This method shows a profile of the bone growing into the channels and the films were used to quantitate the maximum extent of bone penetration. These x-ray films were digitized using a Wild M3C stereomicroscope equipped with a Dage-MTI CCD72 high-resolution videocamera attached to a personal computer equipped with a PixelPipeline frame-acquisition board, and BDS-Oncor image acquisition/analysis software.

The channels, lined by the experimental surfaces and showing bone penetration, were measured end-to-end to determine accurate channel length, and the center of the channel was determined. The furthest extent of bone penetration, from each open end of the channel, was then measured for each channel. Each bone penetration measurement was divided by the distance to the center of the channel. Thus, a measurement of 100% represented full bone penetration from one opening of the channel to the center. Two 100% measurements for one channel meant that bone penetrated the channel from end-to-end.

Tensile Mechanical Testing of the Bone/Implant Interface. Mechanical evaluation was conducted on samples from the chamber model study in order to examine the tensile strength of attachment of ingrown bone to the various surfaces in the study. Each sample consisted of a pair of 7 x 8 mm plates of the experimental materials and the ingrown bone and soft tissue, which formed a 1 x 5 x 8 mm sample between the plates. This "sandwich" was tested in tensile mode to failure in an Instron servohydraulic mechanical testing system by applying tensile force to the top and bottom plates.

The test system consisted of two flat, parallel, attachment surfaces fixed to the servohydraulic actuator and to the load cell. The sample was placed on the lower surface (attached to the load cell) and its lower plate was cemented in place with a small amount of cyanoacrylate cement. The actuator was then lowered and cemented to the upper plate of the specimen. After both plates were cemented firmly the sample was tested in tension at a rate of 10% strain per minute (the crosshead speed was 0.10 mm/min. and the distance between the plates is 1.0 mm) until failure. Failure strength was measured in Newtons.

The cyanoacrylate cement was used because of its high tensile strength, short setting time, and its ability to set in the presence of moisture. Its use allowed rapid testing of fresh specimens without drying. Since the plates of the test specimen were held parallel in the precision-machined polyethylene chambers during bone penetration, they were fixed in parallel position by the ingrown, attached bone. Thus the plates of the removed samples remained rigidly parallel, and the testing was conducted with the plates in parallel orientation. Plate orientation was also routinely evaluated by faxitron imaging. Thus, precision chamber machining and assembly, and the use of precision test fixturing, were utilized to ensure parallel plate orientation during testing.

After testing, the failed specimens were removed from the test fixturing by shearing the plates from the test fixture surfaces, taking advantage of the relatively low shear strength of the cyanoacrylate cement.

In this model the interface tested represented the region between the 5 x 8 mm side of the tissue and the experimental surface. For reference, a 40-N force on this 40-mm^2 sample represented 1 MPa of failure stress if there was bone attachment along the entire interface.

Some samples in each group were saved intact for electron microscopy of the intact bone/implant interface. Some tested samples (with one intact interface remaining) were also processed for electron microscopy in order to examine the failed interface. This provided information on modes of failure.

Imaging of the Implant/Tissue Interface. Intact (untested) chamber model specimens, some mechanically-tested specimens (with one intact interface), and some samples from the IM rod model were dehydrated, embedded in polymethylmethacrylate, and sectioned. Some samples were processed for undecalcified histology while others were polished, and the surfaces were vapor-deposited with a 60 nm layer of carbon.

Some mechanically-tested chamber specimens and IM rod specimens were deproteinated for 30 minutes in 4% sodium hypochlorite (bleach) at pH 11 to remove soft tissue and expose bone mineral and metal structures. These samples were dehydrated, critical point dryed, and vapor-deposited with a 60 nm layer of carbon or sputter coated with a 60 nm layer of gold-palladium.

These samples were examined using a JEOL JSM-T300 scanning electron microscope (Tokyo) equipped with a GW Electronics (Norcross, GA) type 30A backscattered electron imaging system.

Statistical Analysis.
Comparison of all mean values in this study were conducted using Student's *t*-tests, with statistical significance defined as $p \leq 0.05$.

Results.

In Vitro Studies.
Cell Colonization of Blast Textured Culture Surfaces and Smooth Control Surfaces. RTF cells on control (titanium oxide coated and standard culture plates) and textured surfaces showed consistent colonization by day 4 (Fig. 1). Cell outgrowth was observed at the periphery of each "dot," with randomly oriented cells forming circular colonies on these surfaces. As these colonies grew they became confluent with growth occurring at the periphery. Measurements of colony area growth between 4 and 8 days showed that colonization was significantly inhibited on titanium oxide-coated textured surfaces versus flat titanium oxide-coated controls and culture plate controls (Figs. 2 and 3). This area measurement represents colony coverage of the projected surface area and does not take into account the absolute surface area produced by texturing. Thus it is not clear whether this result represents an effect on growth kinetics.

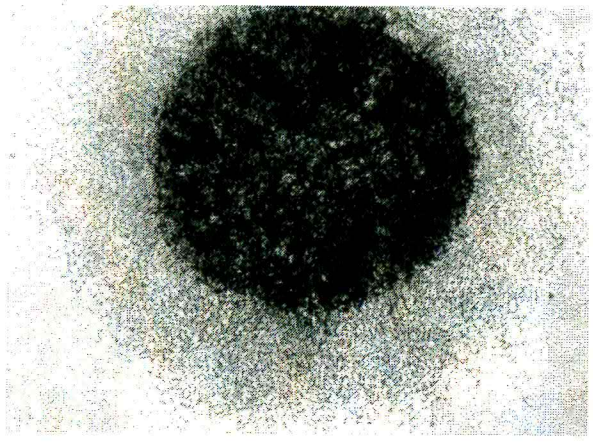

Figure 1. Low power photomicrograph of a stained control cell colony on a culture plate after 4 days in culture. The original collagen dot can be seen as the dark center of the colony. The amount of colony outgrowth can also be seen. The central dot is 2 mm in diameter.

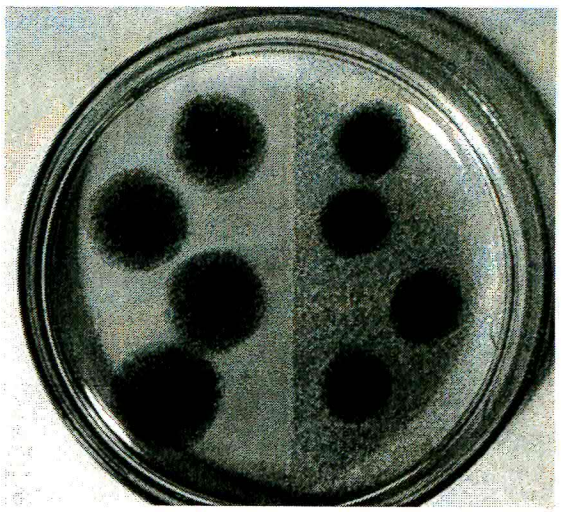

Figure 2. Photograph of stained control cell colonies (left) and colonies grown on a blast-textured area of a 60 mm plate (right), showing differences in colony area at 8 days.

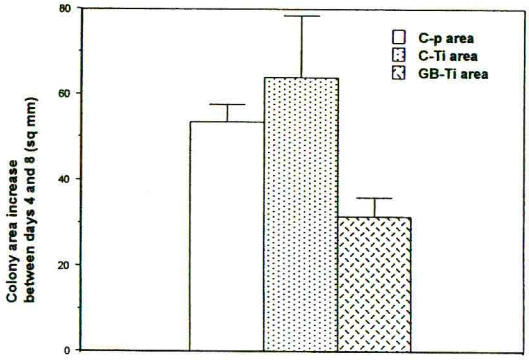

Figure 3. Graph of colony area growth between 4 and 8 days for colonies grown on standard culture plates (C-p) flat titanium oxide coated surfaces (C-Ti) and textured titanium coated surfaces (GB-Ti) showing suppression of growth by the textured surface. Bars represent standard deviation.

Cell Colonization of Microgrooved Culture Surfaces. RTF cells on control surfaces showed growth consistent with the previous experiment. However, colonies grown on the directionally oriented microgrooved surfaces showed preferential colonization (Fig. 4) parallel to the grooves (in the x-axis). The microgrooved surfaces caused elongated colony growth, which was accelerated in the x-direction (parallel to the surface microgeometry) and inhibited in the y-direction (perpendicular to the surface microgeometry). On an individual cell level, the cells were observed to attach

and orient along the surface grooves. This caused the cells to be "channeled" in the x-direction, as compared with control cultures, where the outgrowing cells moved randomly on the flat surfaces. The most efficient cell "channeling" was observed on the 6- and 8-µm surfaces (Fig. 5-7), where cells were observed to attach and orient within the grooves and on flat tops of the grooves (Fig. 8). This resulted in enhanced x-axis growth (Fig. 5) and almost no y-axis growth (Fig. 6) by cells on these surfaces; these cells were spindle-shaped and well-oriented.

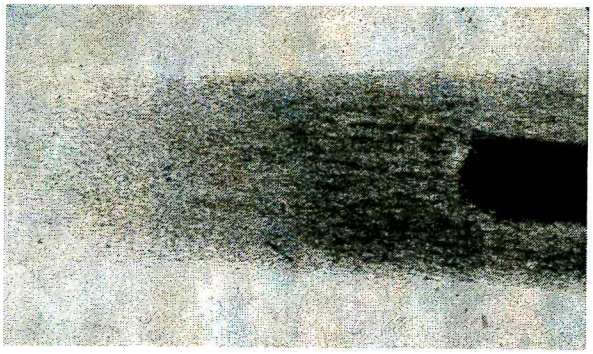

Figure 4. Low power photomicrograph of a stained cell colony on a 6 µm microgrooved plate after 4 days in culture. The grooves, which run horizontally, are too small to be seen at this magnification. The colony shows extensive growth in the x direction (horizontal) and little growth in the y direction.

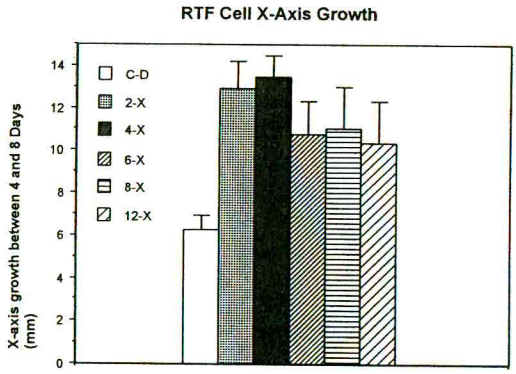

Figure 5. Graphs of X-axis growth by RTF cells on microgrooved surfaces after 8 days compared to control colonies (diameter increase).

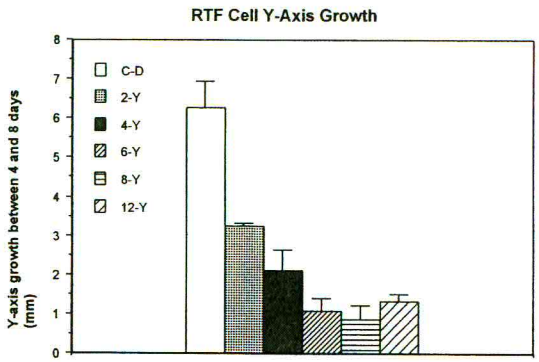

Figure 6. Graphs of Y-axis growth by RTF cells on microgrooved surfaces after 8 days compared to control colonies (diameter increase).

The combination resulted in significant decrease in colony area on the microgrooved surfaces (Fig. 7). On the two smallest microgeometries (Fig. 9) the cells bridged the surfaces of the 2- and 4-µm grooves, resulting in cells with different morphologies than those on the 6-, 8-, and 12-µm surfaces. These cells were more flattened and variably oriented. On the 4-µm grooves the cells showed different mixed morphologies. This resulted in appreciable y-axis growth by the cells on the 2- and 4-µm surfaces. These measurements again represent colony formation on the projected area of the surface and do not take into account that microgrooved surfaces have twice the surface area of flat surfaces.

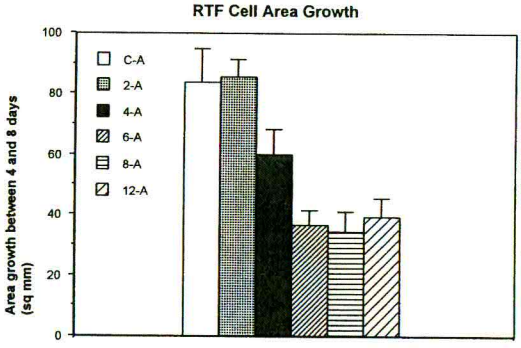

Figure 7. Graphs of colony area growth by RTF cells on microgrooved surfaces after 8 days compared to control colony area growth.

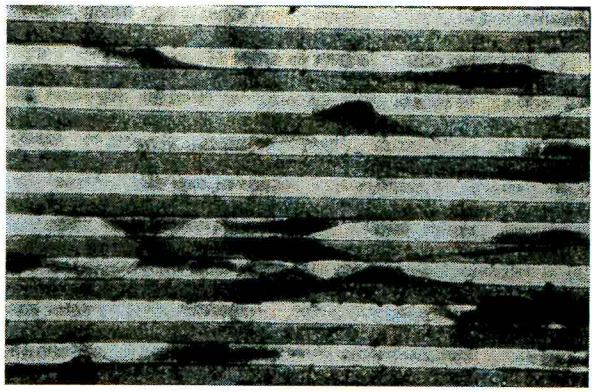

Figure 8. Light photomicrograph of RTF cells growing on a 12 μm microgrooved culture surface. Cells are attached to tops, bottoms, and sides of grooves. Cells are aligned along the long axis of the substrate.

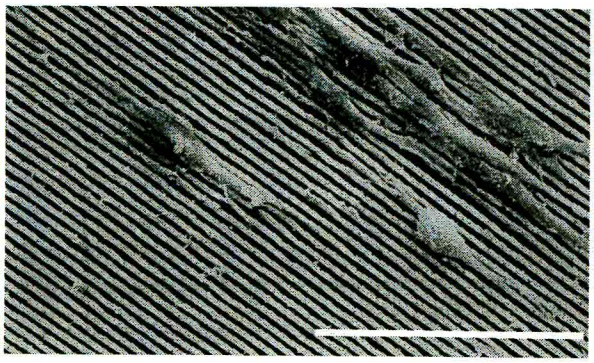

Figure 9. Scanning electron micrograph of RTF cells growing on a 2 μm microgrooved culture surface. Cells are attached to tops of grooves and span several grooves. Cells are aligned along the long axis of the substrate. Bar = 100 μm.

Measurements of cell density on these surfaces (again representing projected area and not real surface area) shows that cell densities on the microgrooved surfaces were similar but lower than those on the control surfaces (Fig. 10). The fact that these measurements represent projected area and not real surface area suggests that cells on the microgrooved surfaces were not utilizing significant amounts of these surfaces. Individual cell attachment areas (Fig. 11) on the microgrooved surfaces were also significantly lower than those on the control surfaces, and cell eccentricities (Fig. 12) were significantly higher. These data suggest that the cells on the microgrooved surfaces were lower in density, less spread, and longer and narrower in shape than those on the control surfaces.

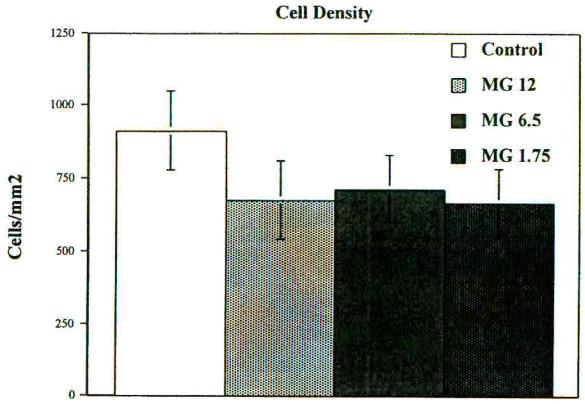

Figure 10. Graphs of cell density (cells/mm^2) on control surfaces and three microgrooved surfaces.

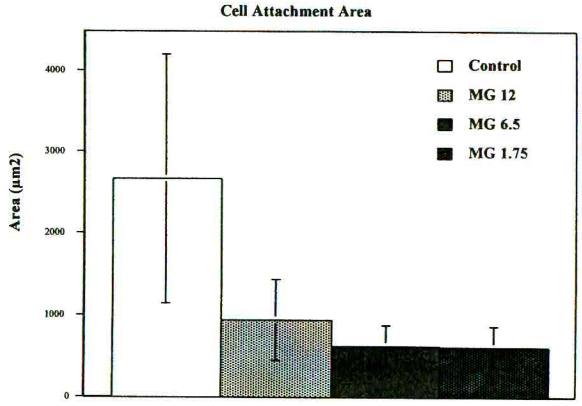

Figure 11. Graphs of cell attachment area (μm^2) on control surfaces and three microgrooved surfaces.

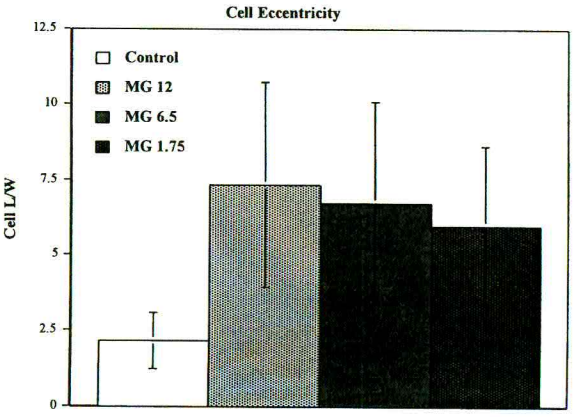

Figure 12 Graphs of cell eccentricity (L/W) on control surfaces and three microgrooved surfaces.

In Vivo Studies.

Laser Microtextured Surface Characteristics. Laser microgrooved surfaces produced by this method were found to be reproducible and consistent. The surfaces showed small amounts of regional variation and could be produced in well defined areas. Figure 13 shows a low magnification scanning electron micrograph (SEM) of a MG12 surface produced on the 1 mm-wide collar of a prototype titanium alloy dental implant. Figure 14 shows a higher magnification SEM of the same surface. The alloy has been ablated from the grooves and deposited in molten form on the ridges between the grooves.

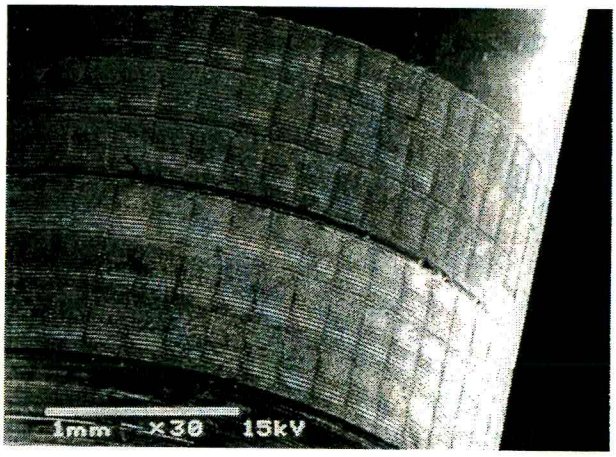

Figure 13. Low power scanning electron micrograph of a prototype dental implant with the upper 1 mm of the collar microtextured with the MG12 surface, and the lower 1 mm portion of the abutment textured as well. Bar = 1 mm.

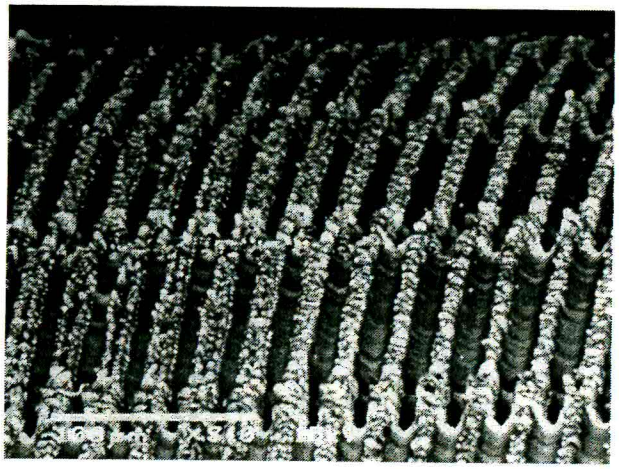

Figure 14. Medium power scanning electron micrograph of a prototype dental implant with the upper 1 mm of the collar microtextured with the MG12 surface. The microgroove pattern, produced in blocks, is shown. Bar = 100 μm.

Implantable Chamber and IM Rod Study Results. Implant chamber model studies showed that canine bone grew into channels lined with the microgrooved surfaces faster and more extensively than in channels lined with blast textured surfaces (Fig. 15). Calcium sulfate also encouraged rapid bone ingrowth with all surfaces (see "Biological Mechanisms of Calcium Sulfate Replacement by Bone"), and the combination of the MG12 surface and calcium sulfate (MG12/CS) produced the most rapid and thorough bone ingrowth of all samples. Note that the microgrooves were oriented parallel to the direction of bone ingrowth. New bone was also observed to attach directly to the MG12 and MG12/CS surfaces (Fig. 16.) and the trabecular bone adjacent to these surfaces was strongly oriented parallel to the microgrooves.

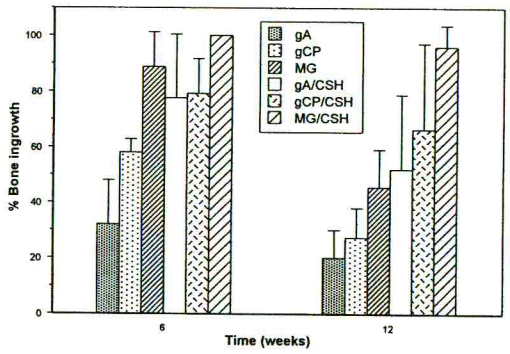

Figure 15. Graph of bone ingrowth into the implantable chamber model showing the effects of the MG surfaces and the CS treatments.

Figure 16. High power light photomicrograph of a bone sample adjacent to a MG12 surface. A small area of attached trabecular bone is shown. The bone has grown into the microgrooves of the surface.

This orientational effect of the MG12 surfaces on attached bone orientation was confirmed in the IM rod samples where orientation of attached bone trabeculae followed microgroove orientation whether it was

circumferential or longitudinal (Figs. 17 and 18). Bone attachment to the MG12 and MG12/CS surfaces was strong enough to measure in tension (Fig. 19) and tensile-tested specimens often showed bone left behind in the microgrooves. Bone surfaces exposed after implant removal always showed extensive bone attachment and growth into the microgrooves (Fig. 18, 20), with trabecular attachments spreading parallel to the microgrooves and blending together to form continuous bands. Electron microscopic results suggested that these surfaces caused orientation of attached cells (Fig. 20), which produced oriented extracellular matrix and oriented bone microstructure. This was not observed on textured surfaces of polished surfaces. Textured surfaces showed moderate direct bone attachment, which was not directional, and the polished surfaces showed little direct bone attachment and mostly fibrous encapsulation (Fig. 21).

Figure 17. Low power scanning electron micrograph of a deproteinated bone specimen from the IM rod study. The implant has been removed, and many small areas of bone attachment to the surfaces are seen. The bone is oriented according to the microgrooving on the implant, which was oriented longitudinally (horizontal) on the right segment and circumferential on the left segment. A 300 μm seam with no microtexturing was in the center. Bar = 1000 μm.

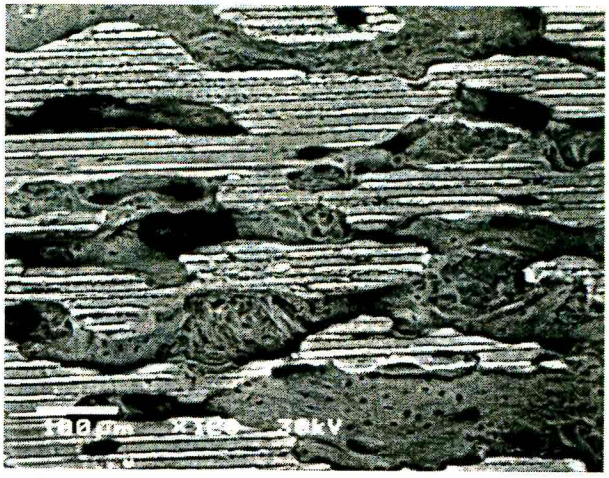

Figure 18. Medium power scanning electron micrograph of a deproteinated bone specimen from the IM rod study. The implant has been removed, and many areas of bone attachment to the surfaces are seen. Bone in these areas shows clear impressions of the implant surface and had grown into the microgrooves. The attachment areas are clearly oriented and elongated parallel to the microgrooves. Several attachments run together to form continuous bands. Bar = 100 μm.

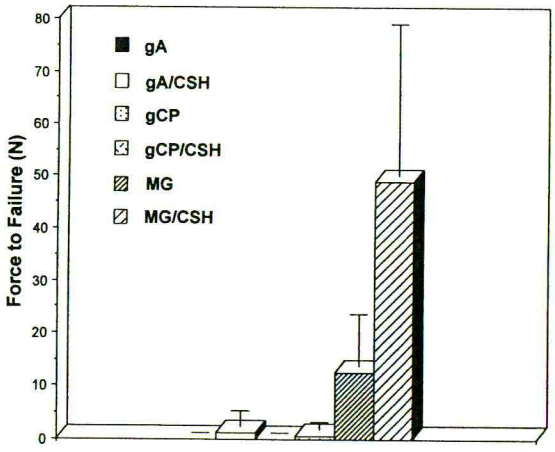

Figure 19. Graph of bone attachment strength (N) showing that only the MG12 and MG12/CS specimens showed measurable tensile attachment to bone.

Figure 20. High power scanning electron micrograph of a deproteinated bone specimen from the IM rod study. The implant has been removed exposing ridges of bone mineral that had been in the microgrooves of the implant. Oriented openings left by cells are visible in the mineral structure.

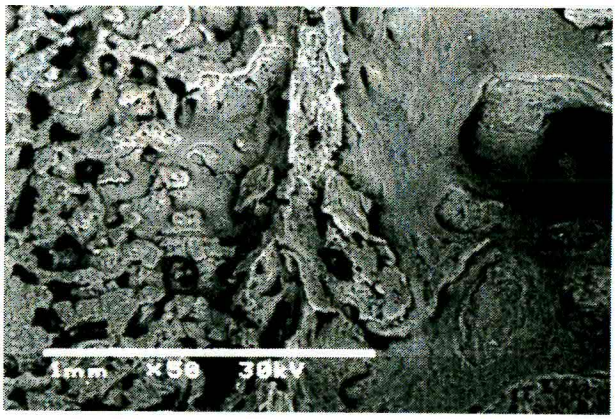

Figure 21. Low power scanning electron micrograph of a deproteinated bone specimen from the IM rod study. The implant has been removed, and many small, randomly-oriented areas of bone contact with a blast-textured implant are seen in the left segment. The bone on the right side had a thick fibrous membrane between it and the polished surface of that segment. There was no direct bone contact in this area. Bar = 1000 μm.

Discussion.

The observed in vitro effects of microgrooved substrates are probably based on the relationship between microgroove size and depth, and the ability of cells to attach, spread, and migrate. Suppression of cell spreading inhibits growth [23] and directs cell migration. The effect of these surfaces on cell attachment, shape, and orientation explains the observed effects on overall colonization. These results are also in agreement with studies that show microgrooves less than 1 μm in depth to be ineffective for the control of tissue integration. Our studies indicate that more than 2 microns of depth are needed for effective cell control. These studies suggest that microgrooved surfaces can not only orient cells and control migration, but also control cell growth to some degree.

The in vivo results can probably be explained at the cellular level based partially on our results showing that fibroblast colonization is inhibited by these surfaces, and also by the results of other showing the effects of textured surfaces on bone cell differentiation [14,15]. On a cellular level microtextured surfaces may suppress early fibrous tissue encapsulation and enhance the differentiation of bone forming cells. Our results are also in agreement with in vitro studies showing that oriented bone cells produce oriented extracellular matrix [24]. Microtexturing of this type probably works on several levels since this type of surface would produce a mechanically stable interface and probably enhance early attachment of fibrin and other proteins [20]

Conclusions.

We have used in vitro methods to survey the effects of a range of microgroove sizes on fibroblast proliferation. Based on these results we have developed laser-microtextured surfaces on metal implants. This method produces surfaces with clean, consistent microstructures, on a micron scale, and can be used to place specific microtextures in highly defined areas. These high-surface-area microtextures show excellent osseointegration and the ability to control the trabecular organization of adjacent bone. They are currently being tested on dental implants and are also being developed for other biomedical applications.

This project was supported by grants from the Orthopaedic Research and Education Foundation, the New Jersey Center for Biomaterials, the New Jersey Commission on Science and Technology, NSF grant DMI-9304020, and NIH grant 1R41 NS351551-01 to Orthogen Corporation.

References

1 Albrektsson T, Brånemark P-I, Hansson H-A, Lindström J. Osseointegrated titanium implants. *Acta Orthop Scand.* 1981; 52: 155-170.

2 Albrektsson T, Hansson H-A, Ivarsson B. Interface analysis of titanium and zirconium bone implants. *Biomaterials.* 1985; 6: 97-101.

3 Albrektsson T, Hansson H-A. An ultrastructural characterization of the interface between bone and sputtered titanium or stainless steel. *Biomaterials.* 1986; 7: 201-205.

4 Haddad RJ Jr, Cook SD, Thomas KA. Biological fixation of porous-coated implants. *J Bone Joint Surg.* 1987; 69A: 1459-1466.

5 Linder L, Albrektsson T, Brånemark P-I, Hansson HA, Ivarsson B, Jonsson U, Lundstrom I. Electron microscopic analysis of the bone-titanium interface. *Acta Orthop Scand.* 1983; 54; 45-52.

6 Linder L, Carlsson A, Marsal L, Bjurstein LM, Brånemark P-I. Clinical aspects of osteointegration in joint replacement: a histologic study of titanium implants. *J Bone Joint Surg.* 1988; 70B: 550-555.

7 Thomas KA, Cook SD. An evaluation of variables influencing implant fixation by direct bone apposition. *J Biomed Mater Res.* 1985; 19: 875-901.

8 Thomas KA, Kay JF, Cook SD, Jarcho M. The effect of surface macrotexture and hydroxylapatite coating on the mechanical strengths and histologic profiles of titanium implant materials. *J Biomed Mater Res.* 1987; 21: 1395-1414,.

9 von Recum AF. Applications and failure modes of percutaneous devices: a review. *J Biomed Mater Res.* 1984; 18: 323:336.

10 Ricci JL, Spivak JM, Blumenthal NC, Alexander H. Modulation of Bone Ingrowth by Surface Chemistry and Roughness. In: Davies, JE ed. *The bone-biomaterial interface.* Toronto: University of Toronto Press; 1991: 334-349.

11 Chehroudi B, Gould TRL, Brunette DM. Effects of a grooved titanium-coated implant surface on epithelial cell behaviour in vitro and in vivo. *J Biomed Mater Res.* 1990; 24: 1067-1085.

12 Inoue T, Cox JE, Pilliar RM, Melcher AH. Effect of the surface geometry of smooth and porous-coated titanium alloy on the orientation of fibroblasts in vitro. *J Biomed Mater Res.* 1987; 21: 107-126.

13 McAuslan BR, Johnson C. Cell responses to biomaterials I: Adhesion and growth of vascular endothelial cells on poly(hydroxyethyl methacrylate) following surface modification by hydrolytic etching. *J Biomed Mater Res.* 1987; 21: 921-935.

14 Batzer R, Liu Y, Cochran DL, Szmuckler-Moncler S, Dean DD, Boyan BD, Schwartz Z. Prostaglandins mediate the effects of titanium surface roughness on MG63 osteoblast-like cells and alter cell responsiveness to 1 alpha,25-(OH)2D3. *J Biomed Mater Res.* 1998; 41(3): 489-496.

15 Kieswetter K, Schwartz Z, Hummert TW, Cochran DL, Simpson J, Dean DD, Boyan BD. Surface roughness modulates the local production of growth factors and cytokines by osteoblast-like MG-63 cells. *J Biomed Mater Res.* 1996; 32(1): 55-63.

16 Brunette DM, Kenner GS, Gould TRL. Grooved titanium surfaces orient growth and migration from human gingival explants. *J Dent Res.* 1983; 62: 1045-1048.

17 Brunette DM. Fibroblasts on micromachined substrata orient hierarchically to grooves of different dimensions. *Exp Cell Res.* 1986; 164: 11-26.

18 Clark P, Connolly P, Curtis ASG Dow JAT, Wilkinson CDW. Topographical control of cell behavior. II. Multiple grooved substrata. *Development.* 1990; 108: 635-644.

19 den Braber ET, de Ruijter JE, Jansen JA. The effect of a subcutaneous silicone rubber implant with shallow surface microgrooves on the surrounding tissues in rabbits. *J Biomed Mater Res.* 1997; 37: (4)539-547.

20 Davies JE. Mechanisms of endosseous integration. *Int J Prosthodont.* 1998; 11(5): 391-401.

21 Spivak JM, Ricci JL, Blumenthal NC, Alexander H. A New Canine Model to Evaluate the Biological Response of Intramedullary Bone to Implant Materials and Surfaces. *J Biomed Mater Res.* 1990; 24(9): 1121-1149.

22 Choueka J, Charvet JL, Koval KJ, Alexander H, James KS, Hooper KA, Kohn J. Canine bone response to tyrosine-derived polycarbonates and poly(L-lactic acid). *J Biomed Mater Res.* 1996; 31: 35-41.

23 Ingber DE, Madri JA, Folkman J. Endothelial growth factors and extracellular matrix regulate DNA synthesis through modulation of cell and nuclear expansion. *In Vitro Cell Dev Biol.* 1987; 23(5): 387-394.

24 Gomi K, Davies JE. Guided bone tissue elaboration by osteogenic cells in vitro. *J Biomed Mater Res.* 1993; 27(4): 429-31.